

# Efficient Computational Design of 2D van der Waals Heterostructures: Band-Alignment, Lattice-Mismatch, Web-app Generation and Machine-learning

Kamal Choudhary<sup>1</sup>, Kevin F. Garrity<sup>1</sup>, Ghanshyam Pilania<sup>2</sup>, Francesca Tavazza<sup>1</sup>

<sup>1</sup> Materials Science and Engineering Division, National Institute of Standards and Technology,  
Gaithersburg, Maryland 20899, USA

<sup>2</sup> Materials Science and Technology Division, Los Alamos National Lab, Los Alamos, New Mexico 87545, United States.

## ABSTRACT

We develop a computational database, web-apps and machine-learning (ML) models to accelerate the design and discovery of two-dimensional (2D)-heterostructures. Using density functional theory (DFT) based lattice-parameters and electronic band-energies for 674 non-metallic exfoliable 2D-materials, we generate 226779 possible heterostructures. We classify these heterostructures into type-I, II and III systems according to Anderson's rule, which is based on the band-alignment with respect to the vacuum potential of non-interacting monolayers. We find that type-II is the most common and the type-III the least common heterostructure type. We subsequently analyze the chemical trends for each heterostructure type in terms of the periodic table of constituent elements. The band alignment data can be also used for identifying photocatalysts and high-work function 2D-metals for contacts. We validate our results by comparing them to experimental data as well as hybrid-functional predictions. Additionally, we carry out DFT calculations of a few selected systems ( $\text{MoS}_2/\text{WSe}_2$ ,  $\text{MoS}_2/\text{h-BN}$ ,  $\text{MoSe}_2/\text{CrI}_3$ ), to compare the band-alignment description with the predictions from Anderson's rule. We develop web-apps to enable users to virtually create combinations of 2D materials and predict their properties. Additionally, we develop ML tools to predict band-alignment information for 2D materials. The web-apps, tools and associated data will be distributed through JARVIS-Heterostructure website (website: <https://www.ctcms.nist.gov/jarvish/>). Our analysis, results and the developed web-apps can be applied to the screening and design applications, such as finding novel photocatalysts, photodetectors, and high-work function 2D-metal contacts.

**Corresponding author:** Kamal Choudhary (E-mail: [kamal.choudhary@nist.gov](mailto:kamal.choudhary@nist.gov))

## 1 INTRODUCTION

Heterostructures are interfaces between dissimilar materials and are of practical importance in a wide variety of optoelectronic devices<sup>1</sup>. Two-dimensional (2D) materials exhibiting van der Waals (vdW) bonding strictly in one of the three crystallographic directions and their heterostructures provide a huge variety of functionality<sup>2, 3</sup> and property-control<sup>4, 5</sup> because their surfaces are generally free from dangling-bonds, extended defects and trap states<sup>6</sup> (which is in stark contrast with semi-coherent and incoherent heterointerfaces found in three-dimensional crystalline solids). Additionally, they allow integrating various nanoscale materials to create diverse vdW heterostructures because they do not require strict constraints of crystal lattice matching<sup>6</sup> and have a wide variety of bandgaps. Despite their widespread applications, a systematic high-throughput investigation of a wide range of 2D chemistries is still lacking, mainly because of the overwhelmingly large number of underlying combinatorial possibilities. The number of possible 2D materials could be in the thousands as shown by recent computational screenings<sup>7-11</sup>, there can be millions of potential pair combinations of distinct heterointerfaces. Moreover, since experimental routes for investigating these heterointerfaces usually are labor and resource-intensive, the use of computational methods, such as density functional theory (DFT), to perform screening is a very well justified first step in an elaborate materials design process.

Metallic 2D materials with high work-functions<sup>12</sup> are useful for battery-applications<sup>13</sup> as well as minimizing Schottky barrier<sup>14</sup>, while 2D semiconducting or insulating materials are good candidates for making different types of heterostructures<sup>15</sup> such as type-I (symmetric), type-II (staggered), and type-III (broken). We determine the types using Anderson's rule, which considers the conduction and valence band information of constituting monolayer only. The information about Conduction Band Minima (CBM) and Valence Band Maxima (VBM) can easily be obtained

from the density functional theory. A type-I band alignment is most widely utilized in optical devices, such as light-emitting diodes (LEDs)<sup>16</sup> and lasers. A type-II band alignment is useful for unipolar electronic device applications, including photodetectors,<sup>17-19</sup> as it can allow for more efficient charge separation and rapid transport for valence and conduction band carriers. The type-III heterostructures are used for tunneling field-effect transistors<sup>20</sup>. Magnetic/non-magnetic heterostructures are also very interesting for proximity-effects during phenomena such as band-tuning<sup>21</sup> and valleytronics<sup>22</sup>. Other important applications of 2D heterostructures include self-cleansing<sup>523</sup>, plasmonic devices<sup>24</sup>, electroluminescence<sup>25</sup>, complementary metal–oxide–semiconductor (CMOS)<sup>26</sup>, and DNA biosensors<sup>6, 27</sup>.

There has been substantial research in the vdW heterostructure design, especially for graphene, BN, black-Phosphorous, and chalcogenides. Some of the highly investigated heterostructures using experimental methods are: WSe<sub>2</sub>/MoS<sub>2</sub><sup>19</sup>, Graphene/MoS<sub>2</sub><sup>27</sup> and WS<sub>2</sub><sup>17</sup>, MoS<sub>2</sub>/h-BN/graphene<sup>28</sup> WSe<sub>2</sub>/CrI<sub>3</sub>.<sup>22</sup> etc. Some of the notable computational works for 2D heterostructure-design include the ones by Ozcelik, et al.<sup>15</sup>, Chiu et al.<sup>29</sup> and Wilson et al.<sup>30</sup>, and Andersen et al.<sup>31</sup>. However, the next generation of 2D materials has gone beyond the known classes and includes many more chemical and structural classes than those investigated in the computational works mentioned above. For a systematic study of heterostructures, a robust algorithm for constructing heterostructures using lattice parameters information and a database of 2D materials' structure and electronic information is essential. Fortunately, recently several computational tools have been developed to identify best-matched configurations including works by Mathew et al.<sup>32</sup>, Dwarkanath et al.<sup>33</sup> based on the algorithm proposed by Zur and McGill<sup>34</sup>. Also, there have been several 2D materials databases that host conduction band minima (CBM), valence band-maxima (VBM), vacuum potentials, and Fermi-energies for 2D materials, such as the JARVIS-DFT<sup>35-39</sup>.

database (<https://www.ctcms.nist.gov/~knc6/JVASP.html>), C2DB<sup>40</sup>, and MARVEL<sup>8</sup>. The easy availability of all the necessary tools for interface design, computational data for 2D materials, and experimental data for validation allows us to investigate a vast majority of all possible combinations of heterostructure chemistries.

Experimentally, 2D-heterostructures are created using manual stacking or direct synthesis using chemical vapor deposition (CVD) processes. Unlike direct CVD growth, whereby vdW heterostructures typically adopt a certain fixed orientation, the manual stacking approach offers a new degree of freedom to tailor the relative alignment (within an error of  $1^\circ$ )<sup>41</sup> between different layers in nearly arbitrary configurations. Moreover, the heterostructures can be created as vertical stacks or as laterally stitched junctions. We consider vertical junctions only in this work. Although 2D heterostructures may not require a strict lattice matching criterion, the presence of sufficient lattice mismatch along with weak vdW bonding between the 2D layers can lead to incoherent lattice matching, and the generation of Moiré patterns<sup>42</sup>.

In this work, we aim to provide an accurate and efficient model to preselect 2D heterostructures for specific applications among a vast pool of candidates. We develop a database and a web interface to facilitate the generation of 2D heterostructures and their classifications. We use the method of Zur et al.<sup>33, 34</sup> to generate interfaces between these 2D materials, and to calculate lattice constants and angle mismatches. The set of 2D materials is obtained from the JARVIS-DFT 2D database, from which we extracted the VBMs, CBMSs, Fermi-energies, equilibrium structures, and wavefunction data. JARVIS-DFT is a database containing about 38000 bulk and 900 low-dimensional materials with their DFT-computed structural, exfoliability<sup>35</sup>, elastic<sup>36</sup>, optoelectronic<sup>37</sup> solar-cell efficiency<sup>39</sup>, and topologically non-trivial<sup>39</sup> properties. It is part of National Institute of Standards and Technology (NIST) effort within the Materials Genome

Initiative (MGI). Next, we develop an easy to use web-app for predicting the heterostructure type and lattice mismatches between all the possible 2D materials in our database. As mentioned above, Anderson’s rule-based designation of heterostructure type requires only the monolayer CBM and VBM of each material. As density functional theory calculations for a vast number of new 2D materials could still be computationally expensive, we could leverage machine-learning (ML) techniques to accelerate the predictions of CBMs and VBMs of 2D materials given the crystal structure information. Hence, we train ML models for conduction band minima (CBM), valence band maxima (VBM) and work-functions of 2D materials using classical force-field inspired descriptors (CFID)<sup>43</sup>. We believe that the easily available heterostructure database along with other calculated properties serves as a useful tool for 2D-heterostructure design.

## 2 METHODOLOGY

DFT calculations were carried out using the Vienna Ab-initio simulation package (VASP)<sup>44, 45</sup> software using the workflow given on our ‘jarvis-tools’ github page (<https://github.com/usnistgov/jarvis>). Please note commercial software is identified to specify procedures. Such identification does not imply recommendation by National Institute of Standards and Technology (NIST). We use the OptB88vdW functional<sup>46</sup>, which gives accurate lattice parameters for both vdW and non-vdW (3D-bulk) solids<sup>35</sup>. The crystal structure was optimized until the forces on the ions were less than 0.01 eV/Å and energy less than 10<sup>-6</sup> eV. The conduction band minima (CBM) and valence band maxima (VBM) are determined based on DFT calculations of monolayers. Also, we calculate the local potential containing ionic plus Hartree and local exchange contributions to determine the vacuum potential (VAC) of a 2D monolayer material. The VAC is subtracted from the VBM and CBM to enable the comparison of band-diagrams of

individual 2D materials in band-alignment diagrams. We use the method of Zur et al.<sup>33, 34</sup> to generate heterostructures of these 2D materials and we calculate the corresponding mismatch of the lattice constants and angles. The implementation is available on our github package, which is adapted from previous works by Mathew et al<sup>32</sup> and Dwarkanath et al<sup>33</sup>. Our implementation of Zur et al.’s method allows easy integration of the database with the available computational-tools at our github page. For two given materials, the band-alignments are determined based on the DFT computations performed using the OptB88vdW method. Based on the band-alignment data their applications and types of heterostructures are determined. We require lattice-mismatch less than/equal to 0.05 % and 1-degree angle tolerance to build the heterostructures. However, we provide all the data and tools to enable users to construct heterostructures with other tighter or looser tolerances. For metallic systems, we determine the workfunction as the difference between the Fermi-energy and the VAC. The web-app is developed using Flask-python<sup>47</sup> and jarvis-tools packages. The Flask-app allows integration of python based-programs and web using very light coding requirements. Finally, we train three regression models for CBMs, VBMs and work-functions. We convert the crystal structure information in terms of Classical Force-field Inspired Descriptors (CFID)<sup>43</sup>, which gives 1557 features for a given input structure. These features include chemical, structural, charge and cell information. We use the gradient boosting decision tree (GBDT) algorithm as implemented in LightGBM<sup>48</sup> to train the models. The CFID descriptors along with GBDT has been shown earlier to generate several high accuracy ML models<sup>43</sup>. We apply variance threshold (threshold = 0.0001) and StandardScaler (zero mean, unity variance) as the preprocessing step on the input features. We use ‘early\_stopping’ during trainings to avoid over-fitting. The optimized parameters for each model are obtained using the randomized search with fivefold cross-validation. We split the whole data in 90 % and 10 % to train and test the data.

After training the models on 90 % data, we evaluate the performance on 10 % held data. As the ML We also perform a five-fold cross-validation study on the whole data to analyze the sensitivity of the selection of dataset-splits.

### 3 RESULTS AND DISCUSSION

We start by employing available JARVIS-DFT data for 2D materials to predict the nature of 2D-heterostructure band alignments. A flow-chart associated with this process is shown in Fig. 1.

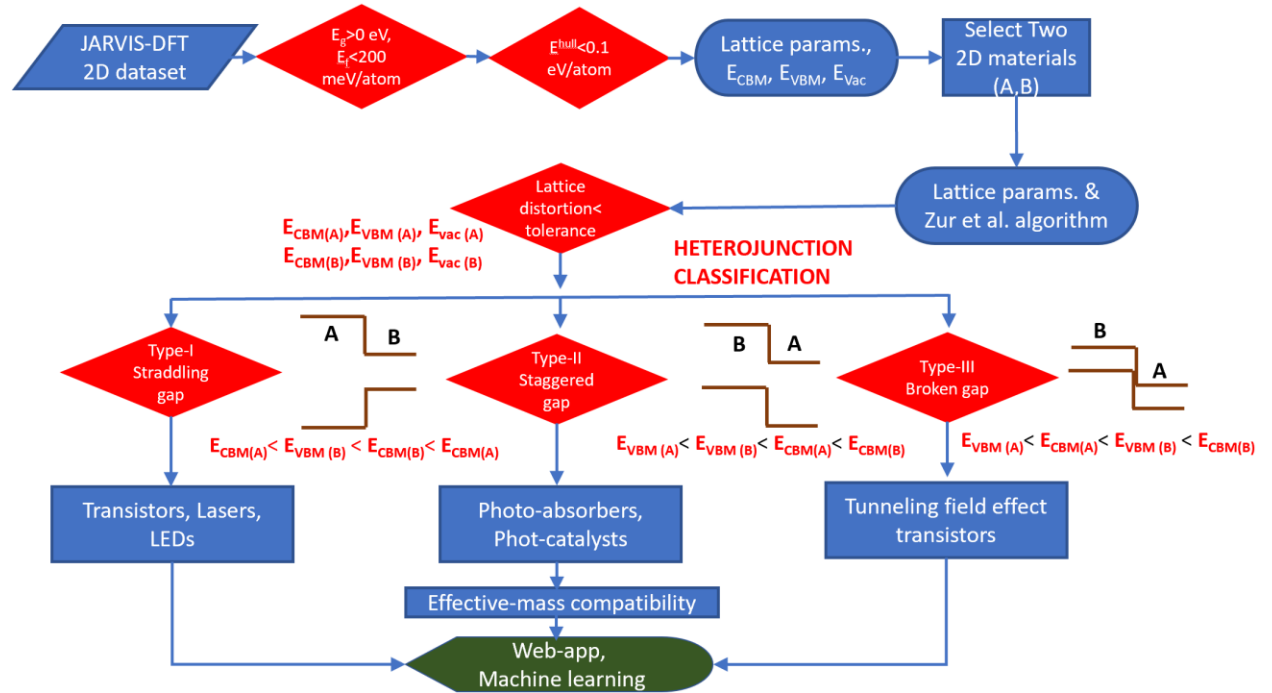


Fig. 1 Flowchart for the computational design of 2D-heterostructures.

The JARVIS-DFT hosts a) DFT-optimized structures and electronic structure information such as b) conduction band minima (CBM), c) valence band maxima (VBM), d) vacuum level information

(VAC). For a heterojunction, we align the 2D materials VBMs and CBMs with respect to corresponding vacuum levels. First, we select non-metallic ( $E_g > 0.0$ ) 2D materials with exfoliation energy less than 200 meV/atom and their bulk counterparts with energy above convex hull less than 0.1 eV/atom, leading to 674 2D materials. The lattice parameter data is then used in finding the best match within angle tolerance of  $1^\circ$  and mismatch of 0.05 % using the algorithm developed by Zur et. al<sup>33, 34</sup>, which finds the heterostructure configuration with the minimal mismatch. Note that we avoid highly mismatched heterostructures because they may lead to the generation of dislocation, grain-boundaries and internal-stress, and other defects that are not included in this work. These heterostructures can be now classified as type-I, type-II, or type-III structures based on the VBM and CBM data mentioned above based on Anderson's rule<sup>49</sup>. A heterojunction is type-I if  $\text{VBM(A)} < \text{VBM(B)} < \text{CBM(B)} < \text{CBM(A)}$ , type-II if  $\text{VBM(A)} < \text{VBM(B)} < \text{CBM(A)} < \text{CBM(B)}$ , and type-III if  $\text{VBM(A)} < \text{CBM(A)} < \text{VBM(B)} < \text{CBM(B)}$ .

Explicit DFT calculations on heterostructures are generally needed to find accurate positions of the electronic states of the heterostructure. Therefore, to assess the accuracy of our predictive approach, we compare the density of states of individual 2D materials, their heterostructure and predicted band-alignment diagrams for a selected set of example materials in Fig. 2. We find that both the  $\text{MoS}_2\text{-WSe}_2$  (JVASP-664-JVASP-652) (Fig. 2a-d),  $\text{MoS}_2\text{-BN}$  (JVAS-664-JVAS-688)- (Fig. 2e-h) and  $\text{MoSe}_2\text{-CrI}_3$  (JVASP-649-JVASP-76195) (Fig. 2i-l) interact feebly, hence the band-alignments predicted using Anderson's rule is similar to the DFT predictions. For instance, the DOS of Mo and S are almost unchanged between pure  $\text{MoS}_2$  and  $\text{MoS}_2$  as part of  $\text{MoS}_2\text{-WSe}_2$  heterostructure (Mo and S DOS in Fig. 2a and 2c are similar). A similar finding applies to both the W and Se DOS. In the resultant heterostructure, the net gap of the system is smaller than both



bandgaps of individual materials, as shown in the band-diagram (Fig. 2d). Similar behavior is also observed for the  $\text{MoS}_2/\text{h-BN}$  and  $\text{MoSe}_2\text{-CrI}_3$  heterostructure.

Similar behavior is also observed for the  $\text{MoS}_2\text{-h-BN}$  and  $\text{MoSe}_2\text{-CrI}_3$  heterostructure. For magnetic/magnetic, magnetic/non-magnetic 2D material interfaces, we predict the band-alignments based on net CBMs and VBMs of both spin channels. Note that the electronic structure of heterostructures with internal stress due to mismatch could be different from that of the two constituent materials, and it would be difficult to predict using the Anderson rule. Ozcelik, et al.<sup>15</sup> reported such behavior for  $\text{MoSe}_2\text{-WSe}_2$  heterostructure. These results also assume that the two 2D-materials do not interact much. However, charge transfer could be possible especially for low-bandgap materials which would change the band-alignment. Note that we discuss intrinsic, defect-free and 0 K results in the current work, while at ambient conditions, equilibrium thermodynamic concentration of defects in systems, and doping levels could also significantly change the heterostructure behavior.

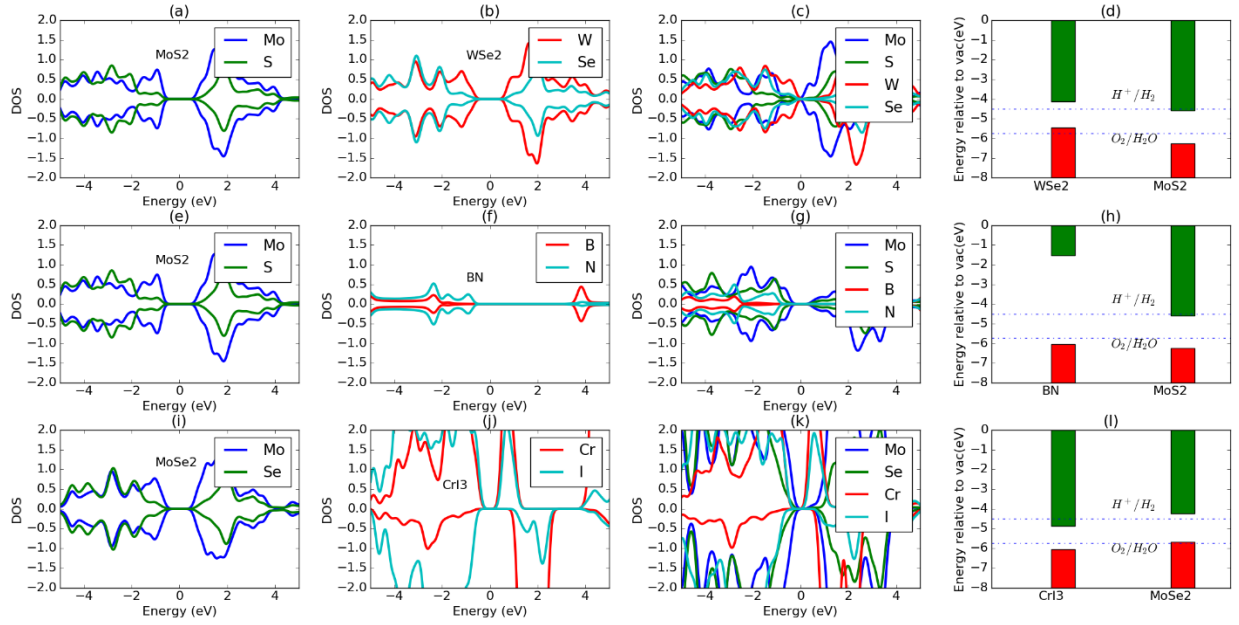


Fig. 2 DFT calculated vs predicted alignments for  $\text{MoS}_2/\text{WSe}_2$ ,  $\text{MoS}_2/\text{h-BN}$ ,  $\text{MoSe}_2/\text{CrI}_3$  heterostructures.

In Fig. 3, we predict the types of all the 226779 heterostructures that we obtained by all possible combinations within the specified lattice mismatch tolerance. Currently, the number of known 2D-heterostructures is in the range of hundreds or thousands, this work suggests thousands to millions of possible heterostructures based on simple combination rules. Each dot in Fig. 3a represents a heterostructure. Fig. 3a shows that it is possible to obtain a variety of heterostructure types for most of the 2D materials. Some materials, however, show a clear preference for a specific heterostructure type. This type of preference is revealed by the appearance of stripes in the Fig. 3a. The stripes are visible mainly for green and red i.e. type-I and type-III heterostructures. As shown in the Fig.3b, we find that the majority of the heterostructures are type-II ( $\approx 37.8\%$ ), the second most are type-I ( $33.4\%$ ), and rarest are type-III ( $28.8\%$ ). This indicates that it is easier to

find 2D heterostructures with photodetector applications than Tunneling Field Effect Transistor (TFET) applications. The number of type-II and type-I are similar, but still, type-II dominates the overall distribution.

We investigate the overall probability that a specific element in the periodic table would form each heterostructure type. Our results are shown in Fig. 4. In order to understand the elemental contributions, we weight an element in both the 2D-systems forming the heterostructure as one or zero separately for the three heterostructures classes (i.e., type-I, II or III heterostructures). After performing such weighting for all the materials in our database, we calculate the probability that an element is part of a particular type of heterostructure. Suppose there are  $x$  number of Se-containing materials and  $y$  of them form type-I heterostructure then the percentage probability ( $p$ ) for Se in type-I is calculated using the formula:  $p = \frac{y}{x} \times 100 \%$ . Interestingly, we find that type-I and type-III heterostructures tend to form with specific elements, while type-II heterostructures are possible with almost all the elements in the periodic table. B, Y, Ru are clearly high-probable for type-I, Rh, Ir, Pt and the group III onwards elements for type-II, and alkali elements and Mn, Fe transition metal elements tend to form type-III heterostructures. Although the periodic table trends provide an overview of the elemental probability, the trends are not obvious and hence there is a need for actual DFT predictions or experiments to confirm the type of the heterostructure. Below we discuss these individual types in further detail and focus on some specific examples where the identified materials can be potentially useful from an application point of view.

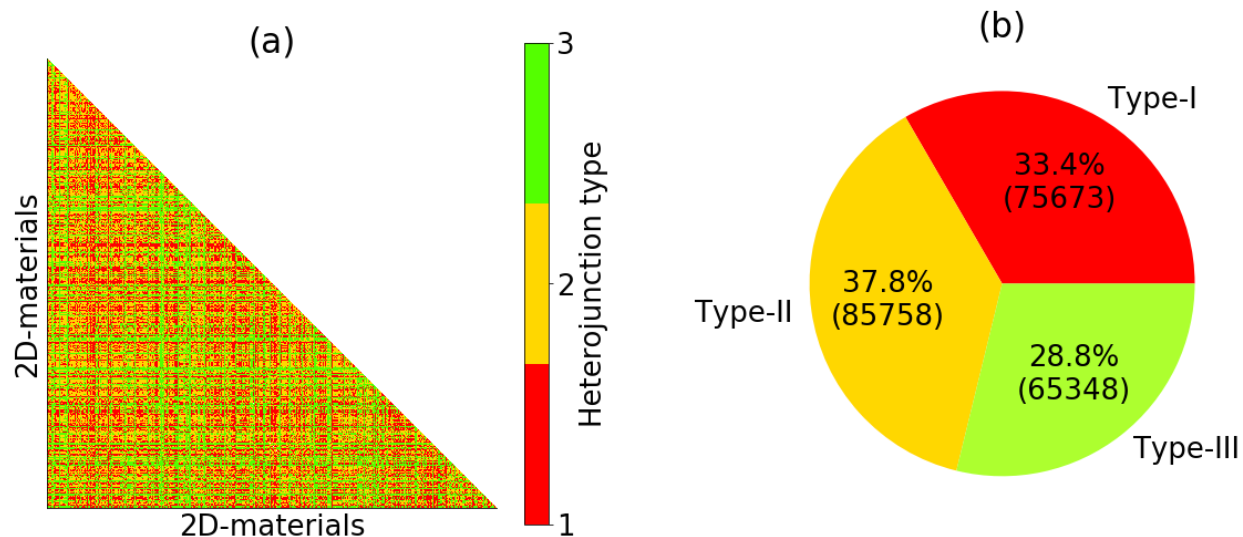


Fig. 3 Distribution of type-I, type-II and type-III heterostructures. a) Combination of all possible heterostructure type for a 2D material. Each point in the plot represents a heterostructure. Each point on x and y axes represents a 2D material. Only the lower diagonal is plotted because it is a symmetric matrix. b) A pie chart of the type-distribution for the three heterostructures.

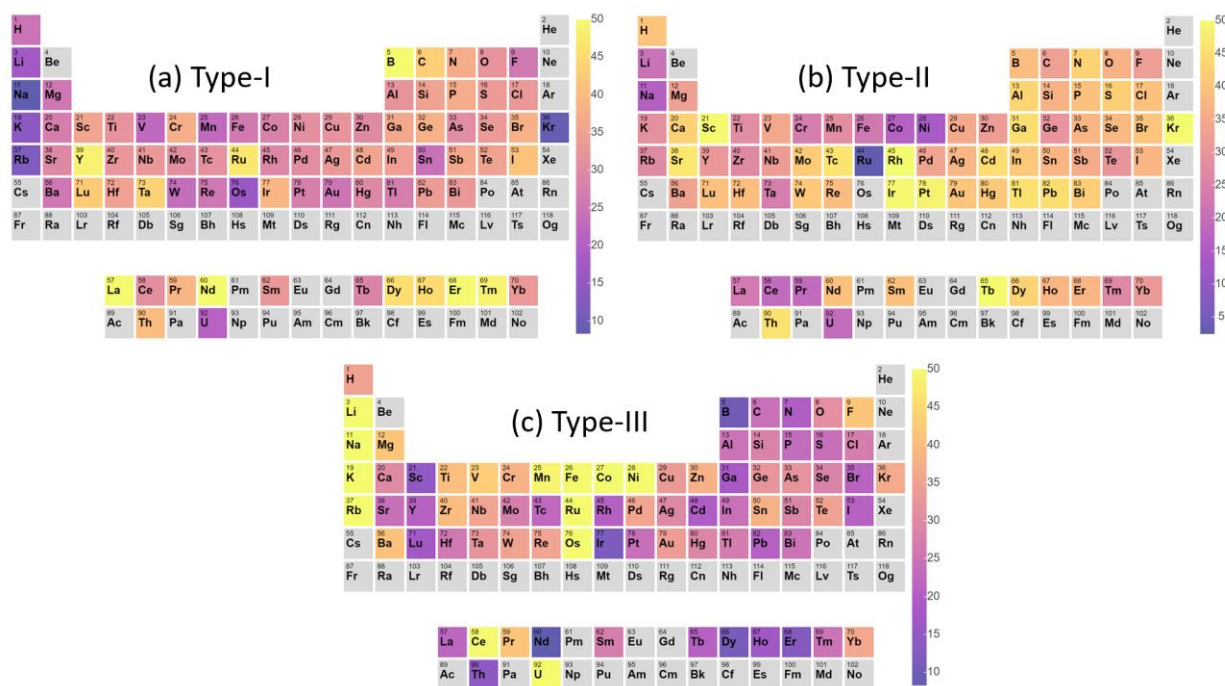


Fig. 4 Periodic table trends of percentage probability that an element is a part of type-I, type-II and type-III heterostructures.

### 3.1 TYPE-I HETEROSTRUCTURE AND OPTOELECTRONICS

Type-I heterostructures are used in transistors, light-emitting diodes (LED) and laser applications<sup>16</sup>. In this case, both the conduction band minimum (CBM) and the valence band maximum (VBM) are located in the material with narrower bandgap. The quantum confinement of electrons and holes in the same region facilitates their radiative recombination, which is desirable in light-emitting applications. An example of such experimentally confirmed type-I materials is  $\text{MoS}_2\text{-ReS}_2$ <sup>50</sup> where  $\text{ReS}_2$  has a narrower gap than  $\text{MoS}_2$ . Using the CBM and VBM datasets, we also find the heterostructure to be type-I, in agreement with the experimental results (shown in the band-alignment diagram in Fig. 5a). Our methodology predicts 21 other 2D-materials that could form type-I heterojunctions with 2H- $\text{MoS}_2$ , such as  $\text{ZrSe}_3$  (JVASP-6019),  $\text{PtSe}_2$  (JVASP-744),  $\text{WS}_2$  (JVASP-652),  $\text{Bi}_2\text{Se}_3$  (JVASP-6736),  $\text{InAg}(\text{PS}_3)_2$  (JVASP-6358),  $\text{SbSI}$  (JVASP-6724), and  $\text{As}_2\text{S}_3$  (JVASP-6451). Therefore, more generally, the computational-tools developed in this work can easily predict all possible potential heterostructures for a given 2D-materials and a specific heterojunction type. Many of these predicted heterostructures are not reported experimentally to the best of our knowledge. Hence, our work could help guide future experiments towards desired heterostructure types.

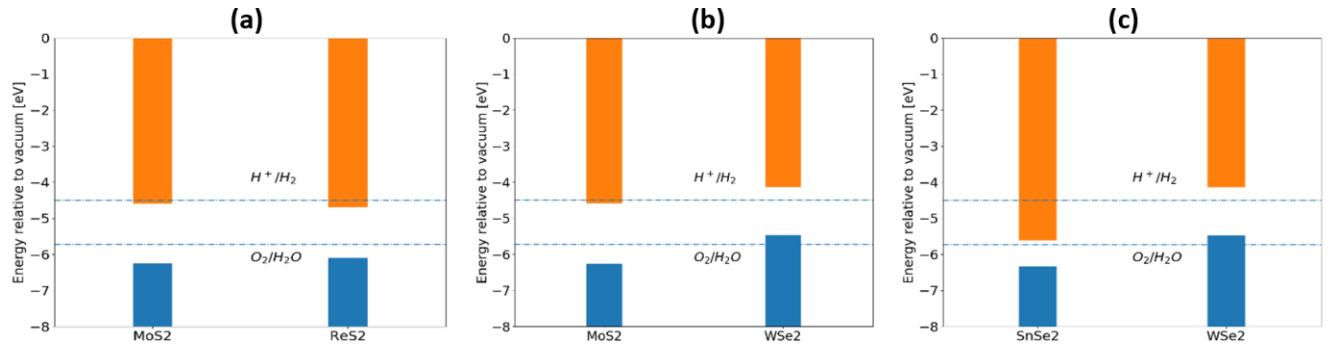


Fig. 5 Examples of type-I, type-II and type-III heterostructure band-alignments. a) 2H- $\text{MoS}_2/\text{ReS}_2$ , b)  $\text{MoS}_2/\text{WSe}_2$ , and c)  $\text{SnSe}_2/\text{WSe}_2$  interface. The dotted lines show the  $\text{H}^+/\text{H}_2$  and  $\text{O}_2/\text{H}_2\text{O}$  levels that could be used for photocatalysis applications.

### 3.2 TYPE-II HETEROSTRUCTURE AND PHOTODETECTION/ABSORPTION

In type-II materials, the CBM and VBM of the resultant structure are located in two different materials. The excitation of the wide-gap material is followed by the transfer of electrons, but not the holes. The opposite charge transfer occurs when the narrow-gap material is excited. The separation of the electrons and holes to different layers can increase their lifetime and is desirable for photovoltaics and photodetection applications. A well-known example of type-II 2D heterostructure is MoS<sub>2</sub>/WSe<sub>2</sub> interface<sup>51</sup>. Using our methodology, we predicted this system to be type-II as well, which once again validates our approach (Fig. 5b). The CBM resides in MoS<sub>2</sub> while the VBM in WSe<sub>2</sub>. In this case, upon irradiation, photons are absorbed, and excitons are generated in the single-layers of WSe<sub>2</sub> and MoS<sub>2</sub>. The photo-generated free electrons in the CBM of WSe<sub>2</sub> can be transferred to the CBM of MoS<sub>2</sub> owing to the large band offset between WSe<sub>2</sub> and MoS<sub>2</sub>. Therefore, compared to the single-layer materials, the heterojunction leads to a better utilization of light and provides more electrons for the reaction, therefore increasing PEC current up to ~6 times compared to single 2D materials<sup>51</sup>. As an example, we predict 43 2D materials that could form type-II heterojunction with 2H-MoS<sub>2</sub> including GaTe (JVASP-6838), MoSe<sub>2</sub> (JVASP-649), CrBr<sub>3</sub> (JVASP-6088), Sb<sub>2</sub>S<sub>3</sub> (JVASP-6523).

### 3.3 TYPE-III HETEROSTRUCTURE AND TFETS

Lastly, in type-III heterojunctions, the band-edges do not overlap at all, making the overall heterojunction metallic. The situation for carrier transfer is like type-II, just more pronounced. Type-III heterojunctions are used in tunneling field-effect transistors (TFETs). TFETs could be

used to mitigate the issue of conventional metal–oxide–semiconductor field-effect transistors (MOSFETs) due to scaling down the supply voltage with the increasing power density and the thermionic emission limitation of carrier injection<sup>52, 53</sup>. Unlike type-I and II, there are very few type-III heterojunctions known<sup>52</sup>. An experimentally known example of type-III heterojunction is SnSe<sub>2</sub>/WSe<sub>2</sub><sup>52</sup>(JVASP-762, JVASP-652) which we also find as type-III (Fig. 5c). As an example, screening for 2D materials that can form type-III with 2H-MoS<sub>2</sub>, we find MnO<sub>2</sub> (JVASP-6922). Similarly, searches for all the possible combinations could be performed to guide computations or experimental work.

### 3.4 WATER-SPLITTING

2D-materials can be used for water-splitting to generate H<sub>2</sub> and O<sub>2</sub> gases when irradiated with sunlight<sup>54, 55</sup>. For a material to be able to split water, its CBM must lie at a more negative potential than the reduction potential (H<sup>+</sup>/H<sub>2</sub>: 0.0 eV vs. Normal hydrogen electrode (NHE) at pH 0) and the valence band maximum must exhibit more positive potential than the oxidation potential (O<sub>2</sub>/H<sub>2</sub>O: +1.23 eV vs. NHE at pH 0). Out of all the 2D materials in our database, we could find 180 2D monolayer materials that satisfy this condition as shown in Fig. 6. Some of the materials are already known water splitters, including BN<sup>56</sup>, black-P<sup>54</sup>, ZnPS<sup>357</sup>), but many other materials, including As<sub>2</sub>O<sub>3</sub>, InSe, HfBrN, and ZnSiO<sub>3</sub> are not known experimentally as photocatalysts for water-splitting. As the band-edges could be tuned using different types of 2D materials, the heterostructures would allow a greater number of materials with water-splitting capabilities. Also, a heterostructure, especially of type-II as discussed above, can prevent electron-hole pairs (EHP) from recombining by separating the electrons and holes, which would increase the photogeneration rate.

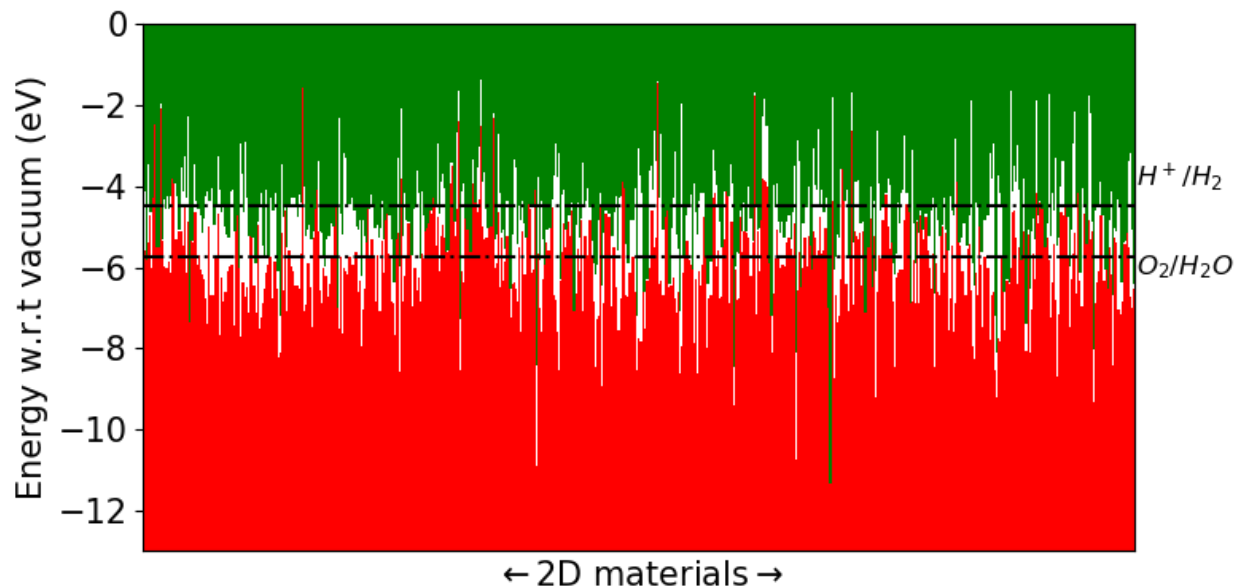


Fig. 6 Band-diagrams of the non-metallic 2D materials with respect to  $H^+/H_2$  and  $O_2/H_2O$  levels.

### 3.5 HIGH WORK-FUNCTION 2D -MATERIALS

Heterostructures, which utilize 2D materials as metallic contacts instead of conventional metallic contacts such as Al, Pt and Cu are of great importance in designing electronic devices. But very few such 2D materials with high work function (WF) have been reported<sup>12-14</sup>. These materials have been shown to act as an excellent contact for 2D heterostructures and could be advantageous compared to conventional contacts such as Pt because of easier lattice mismatch. In Fig. 7, we show the WF distributions for all the 2D metals. We observe that most of the WFs are centered around the 4 eV to 5 eV window, but high WFs are also possible. Some of the high work-function 2D-metals are:  $WO_2$  with 9.6 eV (JVASP-783),  $MoO_2$  with 9.3 eV (JVASP-78036),  $TiO_2$  with 8.77 eV (JVASP-765),  $ZrN_2$  with 7.07 eV (JVASP-75043),  $PtCl_2$  with 6.96 eV (JVASP-28136) etc. As expected, most of the high workfunction 2D materials are oxides.



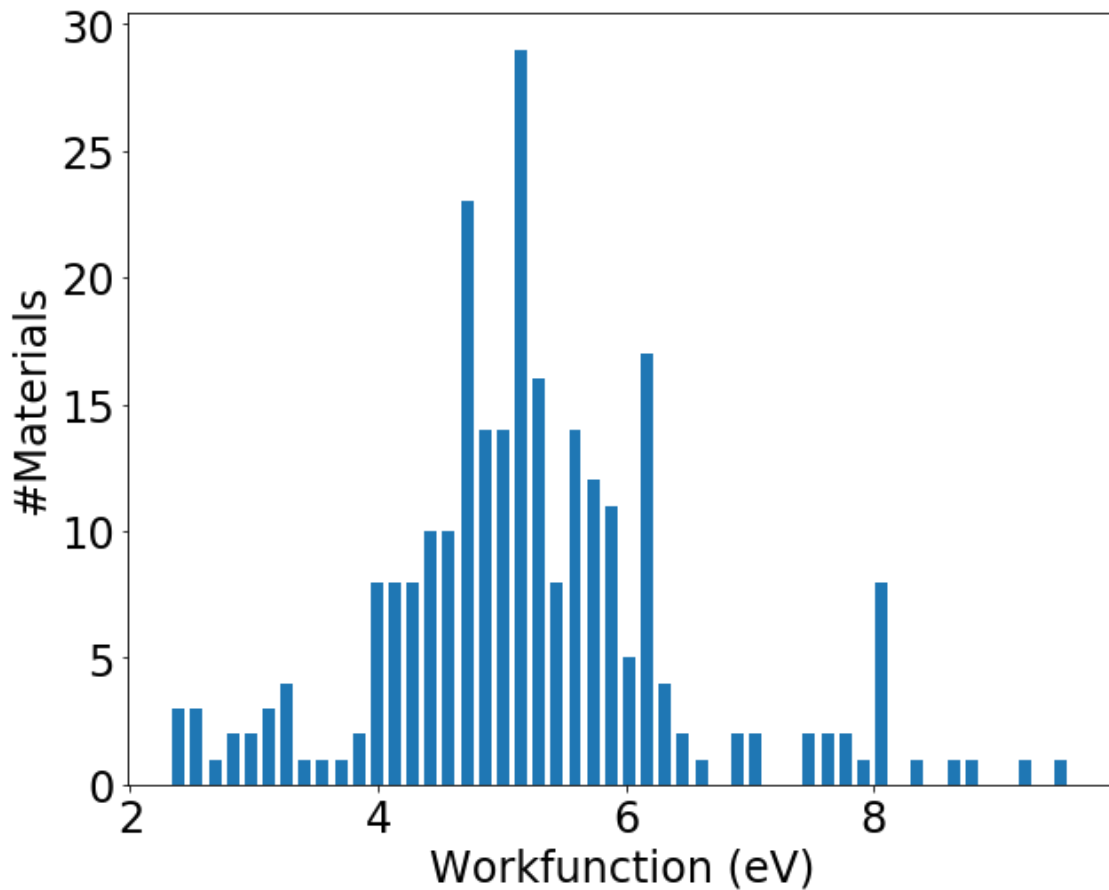


Fig. 7 Workfunction distribution of 2D metals.

### 3.6 WEB-APPS

We now describe the details of the developed website application (web-app), which is specifically designed to facilitate easy predictions and further analysis of 2D-heterostructure. A snapshot of the *JARVIS-Heterostructure app* is shown in Fig. 8. In this app, the electronic bands data and lattice-matching algorithm are used to predict the possible 2D heterostructure and its type. Currently, there are two sub-apps: a) a user can select options of two 2D materials (for which

computed data is already available for 2D materials) to predict the lattice-mismatch and band-alignments of the heterostructures, b) computationally design a heterostructure for arbitrary 2D materials. The possible options are all the semiconducting 2D materials in the database. In addition to the mismatch and band-alignment information, the app shows the band-diagram to help visually analyze the results. In case some material is not in the database, the user can put two 2D materials crystallographic information in the second app, which then makes the 2D heterostructure under the pre-defined mismatch criteria. The user can then run the calculations on the three structures to predict the heterostructure properties. The code to generate band-alignments and the heterostructure is freely available at the jarvis-tools github page (<https://github.com/usnistgov/jarvis>). The web-app will be made available at: <https://www.ctcms.nist.gov/jarvish>.

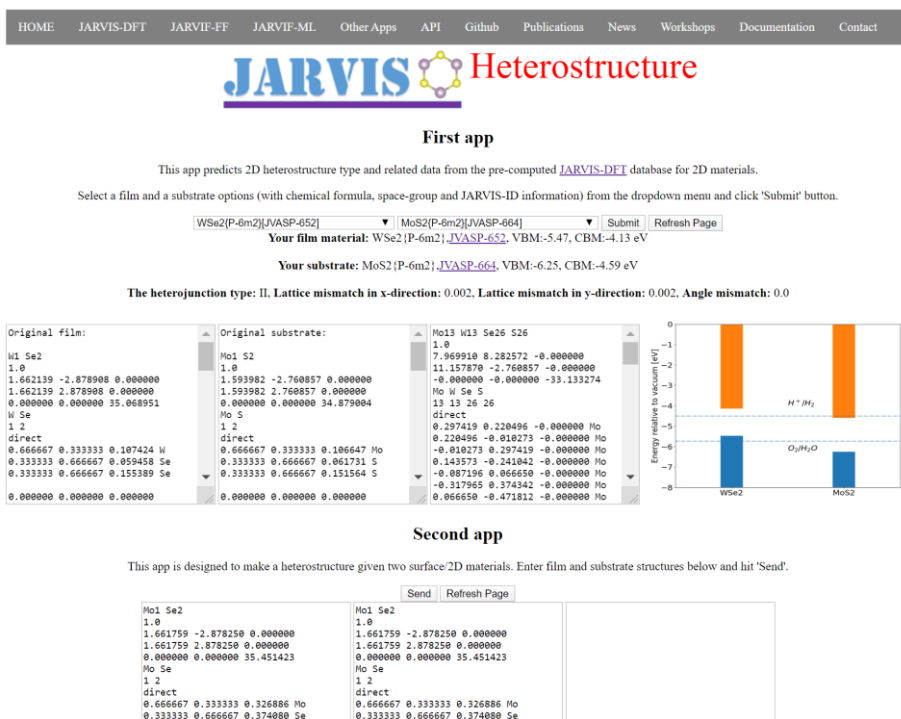


Fig. 8 Snapshot of the JARVIS-Heterostructure app showing two sub-apps.

### 3.7 MACHINE-LEARNING APPLICATIONS

To treat possible 2D materials that are not yet in our database, we develop machine-learning (ML) models for the band diagrams of 2D materials. For all the 2D materials under investigation, we convert the crystal structures into 1557 Classical Force-field inspired Descriptors (CFID) descriptors as the input data, we consider CBMs, VBMs, and workfunctions (WFs) from the JARVIS-DFT calculation results as the target data for ML. In the Fig. 9a-c we visualize the target data distribution. This helps us understand the boundaries in which the ML algorithm would work well, as ML algorithms are good for interpolation purposes only and generally fail at extrapolation. We develop three regression models using the gradient boosting decision tree algorithm as implemented in LightGBM<sup>48</sup>. After the preprocessing steps, the number of features reduces from 1557 to 1497, suggesting that a few of the 1557 features were correlated, and only unique features are kept. The number of optimized trees during the ‘early\_stopping’ and optimized parameters differ in each model. After obtaining the optimized parameters with hyperparameter optimization, we evaluate the performance on 10% held test data which is never used during training or finding hyperparameters. The results of this test are shown in Table. 1. As it is possible that a 90 % and 10 % split could be biased; therefore, we perform five-fold cross-validation on each model with complete data. We report the corresponding mean absolute error and standard deviations as shown in the Table. 1 as well. In Fig. 9d-f we show the DFT vs ML predictions after training the GBDT algorithm on 90 % training data and testing on 10 % held data. The results for the trained models are given in the Table. 1 and clearly suggests that for most of the models we achieve reasonable-accuracy compared to the average-predicting baseline model and the models could be used on new materials which are not currently available in our database. On the second app discussed above,

we plan to integrate the ML models so that users can input crystal structure and find the best-matched interface as well as get ML predictions for the heterostructure design.

*Table. 1 Machine-learning model performance using Mean Absolute Error (MAE) as a metric.*

*Mean and standard deviation values are shown for 5-fold cross-validation (CV) results also.*

Model	MAE (Test-set)	Baseline MAE	5-fold CV MAE
<b>VBM (eV)</b>	0.67	1.47	0.67 $\pm$ 0.13
<b>CBM (eV)</b>	0.62	1.07	0.61 $\pm$ 0.15
<b>Work-function (eV)</b>	0.54	0.95	0.54 $\pm$ 0.18

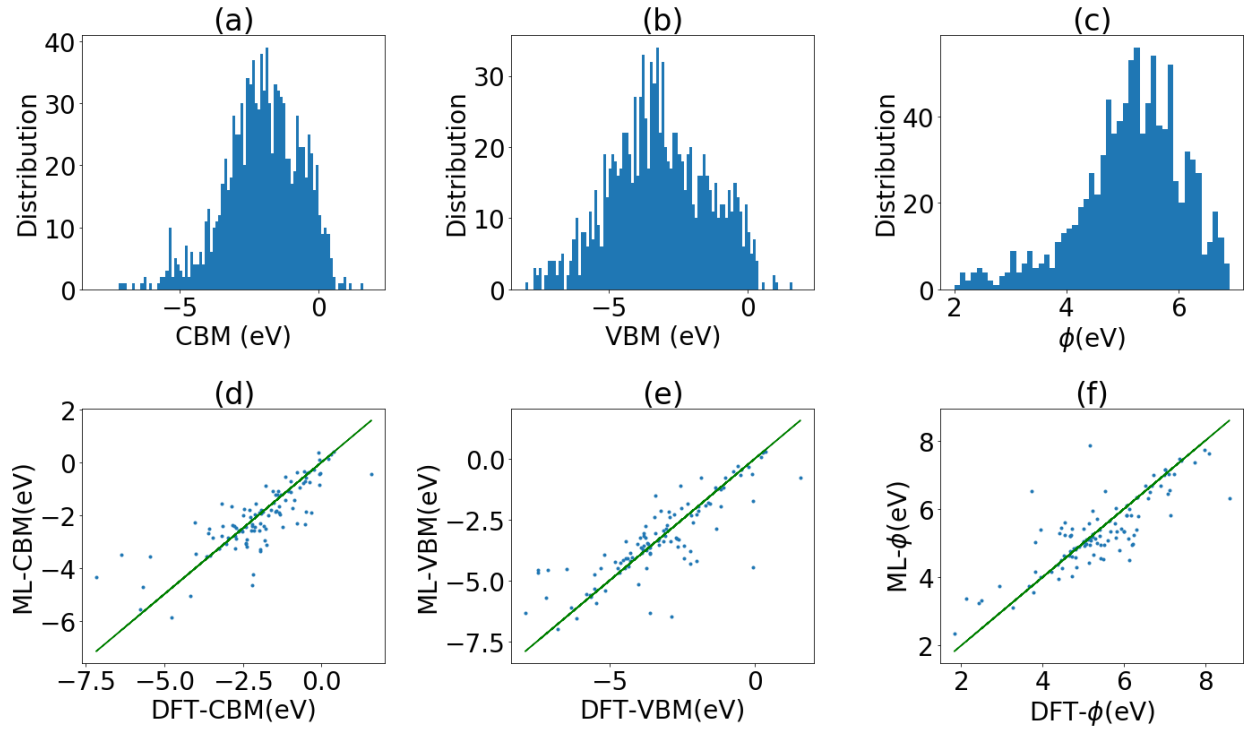


*Fig. 9 Data-distribution and ML performance on the 10 % held set of 2D materials.*

### 3.8 LIMITATIONS

Although the above tools and datasets provide a unique resource for predicting 2D heterostructures, there are various limitations that we mention here. First, the conventional semi-local DFT functionals we use in this work are known to underestimate the bandgaps of materials<sup>58</sup>. Higher levels methods such as hybrid-functionals<sup>59, 60</sup>,  $G_0W_0$ <sup>61, 62</sup> Bethe-Salpeter (BSE)<sup>63</sup> are needed to correct this issue, however, they are computationally very expensive. It is important to check the accuracy of the band-edge positions of the OptB88vdW with respect to HSE06 type methods. The OptB88vdW is taken from the JARVIS-DFT while the PBE and HSE06 data are taken from Ozcelik, et al.<sup>15</sup> for 14 materials such as BN, 2H-MoS<sub>2</sub>, 1T-HfS<sub>2</sub>. In Fig. 10, we compare the band-edges of 14 2D materials obtained from OptB88vdW with respect to PBE and HSE06 functionals. The Pearson correlation coefficient is used to find the relationship of data from different DFT methods. We find that the PBE and OptB88vdW band-edges adjusted with respect to the vacuum level of each material are very similar, with PC more than 0.96 for both CBMs and VBMs. This indicates that the conventional DFT method based heterostructure predictions should be comparable among themselves. Next, we compare the band-edges with respect to HSE06. Surprisingly, we find that the CBMs of the two functionals are highly correlated while the VBMs are less correlated with deviations mainly attributed to nitride class of materials such as BN and AlN.

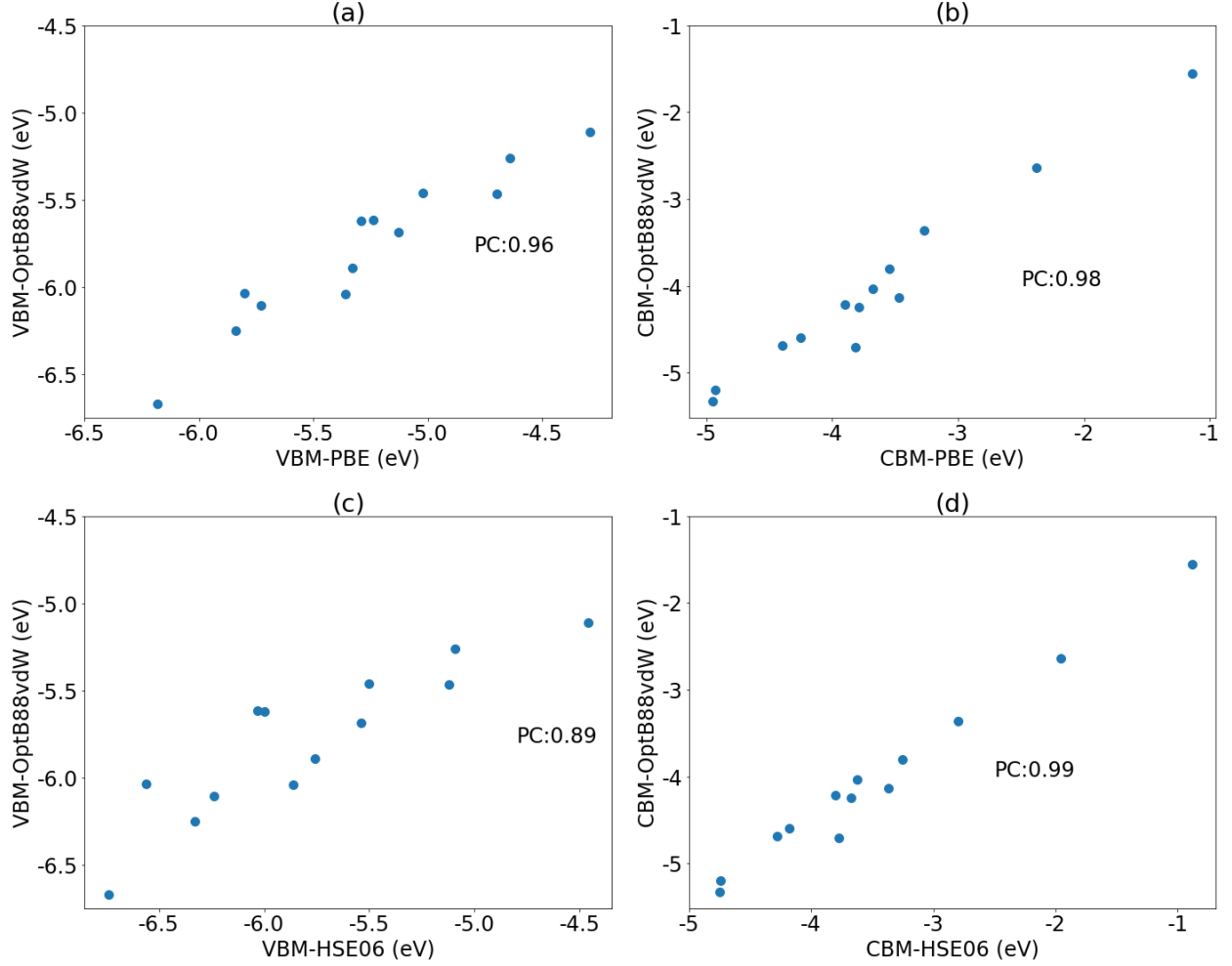


*Fig. 10 Comparison of OptB88vdW conduction band minima (CBM) and valence band maxima of a few 2D materials with that obtained from PBE and HSE06 functionals.*

In addition to the bandgap, it is important to consider the selective optical transitions in the vdW heterostructures, and carrier effective mismatches. For many of our 2D materials, we report the effective mass of individual 2D materials with the help of BoltzTrap code. Examples of using this code are given in our github page. The effective masses of the both the 2D materials in a heterostructure should be comparable because the carriers from the VBM/CBM of one material would jump to the CBM/VBM of another and it is important that the carriers encounter a similar band-structure, hence also the similar effective masses. Distribution of the effective mismatches

of 2D heterostructures in Fig. 11 shows that the majority of the heterostructures have negligibly small effective mass-mismatches with the highest ones up to  $4m_e$ . This suggests that most of the heterostructures would have effective mass compatibility. Note that computational data of effective masses for 2D materials are available for the majority of systems in our database, but for the systems where such information is not available, subsequent calculations could be necessary for heterostructure designs. It is also important to check if the optical transitions are allowed based on the symmetry of the 2D materials, and generally requires optical property calculations for heterostructures, which is beyond the scope of present work. For example, in Fig. 2c and Fig. 2d, the DFT calculations or band-diagrams could only provide the information whether there could be allowed electronic states. It does not provide the information on whether electronic transitions are allowed based on the symmetry of the wavefunctions. Nevertheless, we believe the tools and data would be useful for the initial selection of heterostructures.

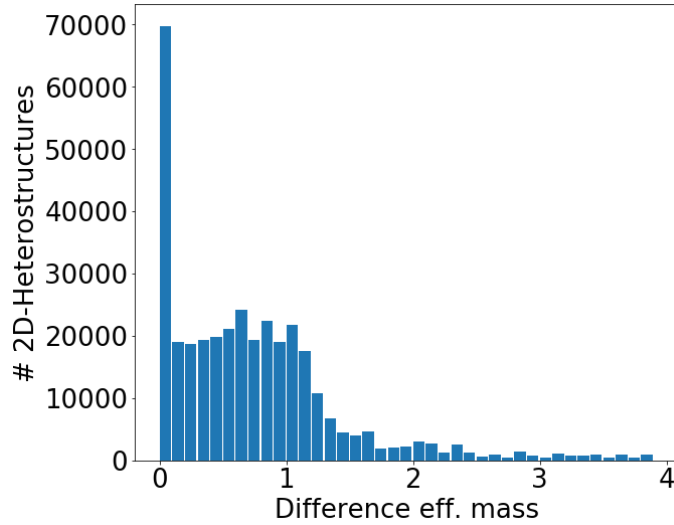


*Fig. 11 Difference in effective mass distributions for 2D-heterostructures.*

## 4. CONCLUSIONS

We present a computational database, tools, web-apps and machine-learning models to accelerate the design and discovery of 2D-heterostructures. Using lattice-parameter and density functional theory (DFT) based electronic level information of 674 non-metallic 2D-materials, we generate 226779 heterostructures and classify them into type-I, II and III systems according to Anderson's rule. We find that type-II is the most common and the type-III the least common heterostructure type. We analyze the chemical trends of all the generated heterostructures in terms of the periodic table of constituent elements and identify which atomic constituents are more likely to form low-mismatch and a particular type of heterostructures. The band alignment data can also be used for finding photocatalysts and high-work function 2D-metal contacts. We validate our results with respect to experimental data for a few systems and compare the electronic levels with respect to hybrid-functionals. Additionally, we carry out explicit DFT simulation of a few selected heterostructures, to compare the band-alignment description with the predictions from Anderson's rule. Finally, we develop web-apps and machine-learning models to enable users to virtually create combinations of 2D heterostructures and predict their properties.

## ACKNOWLEDGEMENTS

K.C., K.F.G., and F.T. thank National Institute of Standards and Technology for funding, computational and data-management resources (NIST-Raritan, and NIST-CTCMS). K.C. also thank the computational support from XSEDE computational resources under allocation number (TG-DMR 190095). G.P. would like to acknowledge support from the Los Alamos National Laboratory's Laboratory Directed Research and Development (LDRD) program's Directed Research (DR) project #20200104DR. Los Alamos National Laboratory is operated by Los



Alamos National Security, LLC, for the National Nuclear Security Administration of the (U.S.)  
Department of Energy under contract DE-AC52-06NA25396.

## REFERENCES

1. Agostini, G.; Lamberti, C., *Characterization of semiconductor heterostructures and nanostructures*. Elsevier: 2011.
2. Wang, X.; Xia, F., Van der Waals heterostructures: Stacked 2D materials shed light. *Nature Materials* **2015**, *14* (3), 264.
3. Li, M.-Y.; Chen, C.-H.; Shi, Y.; Li, L.-J., Heterostructures based on two-dimensional layered materials and their potential applications. *Materials Today* **2016**, *19* (6), 322-335.
4. Liu, Y.; Weiss, N. O.; Duan, X.; Cheng, H.-C.; Huang, Y.; Duan, X., Van der Waals heterostructures and devices. *Nature Review Materials* **2016**, *1* (9), 16042.
5. Sun, Z.; Martinez, A.; Wang, F., Optical modulators with 2D layered materials. *Nature Photonics* **2016**, *10* (4), 227.
6. Novoselov, K.; Mishchenko, A.; Carvalho, A.; Neto, A. C., 2D materials and van der Waals heterostructures. *Science* **2016**, *353* (6298), aac9439.
7. Choudhary, K.; Kalish, I.; Beams, R.; Tavazza, F., High-throughput Identification and Characterization of Two-dimensional Materials using Density functional theory. *Scientific Reports* **2017**, *7* (1), 5179.
8. Mounet, N.; Gibertini, M.; Schwaller, P.; Campi, D.; Merkys, A.; Marrazzo, A.; Sohler, T.; Castelli, I. E.; Cepellotti, A.; Pizzi, G., Two-dimensional materials from high-throughput computational exfoliation of experimentally known compounds. *Nature Nanotech.* **2018**, *13* (3), 246-252.
9. Cheon, G.; Duerloo, K.-A. N.; Sendek, A. D.; Porter, C.; Chen, Y.; Reed, E. J., Data mining for new two-and one-dimensional weakly bonded solids and lattice-commensurate heterostructures. *Nano Lett.* **2017**, *17* (3), 1915-1923.
10. Ashton, M.; Paul, J.; Sinnott, S. B.; Hennig, R. G., Topology-scaling identification of layered solids and stable exfoliated 2D materials. *Phys Rev. Lett.* **2017**, *118* (10), 106101.
11. Zhou, J.; Shen, L.; Costa, M. D.; Persson, K. A.; Ong, S. P.; Huck, P.; Lu, Y.; Ma, X.; Chen, Y.; Tang, H., 2DMatPedia, an open computational database of two-dimensional materials from top-down and bottom-up approaches. *Scientific Data* **2019**, *6* (1), 86.
12. Chuang, S.; Battaglia, C.; Azcatl, A.; McDonnell, S.; Kang, J. S.; Yin, X.; Tosun, M.; Kapadia, R.; Fang, H.; Wallace, R. M., MoS<sub>2</sub> p-type transistors and diodes enabled by high work function MoO<sub>x</sub> contacts. *Nano Lett.* **2014**, *14* (3), 1337-1342.
13. Jing, Y.; Zhou, Z.; Cabrera, C. R.; Chen, Z. J. T., Metallic VS<sub>2</sub> monolayer: a promising 2D anode material for lithium ion batteries. *J. Phys. Chem. c* **2013**, *117* (48), 25409-25413.
14. Farmanbar, M.; Brocks, G., Controlling the Schottky barrier at MoS<sub>2</sub>/metal contacts by inserting a BN monolayer. *Phys. Rev. B* **2015**, *91* (16), 161304.
15. Özcelik, V. O.; Azadani, J. G.; Yang, C.; Koester, S. J.; Low, T., Band alignment of two-dimensional semiconductors for designing heterostructures with momentum space matching. *Phys. Rev. B* **2016**, *94* (3), 035125.
16. Nakamura, S.; Senoh, M.; Iwasa, N.; Nagahama, S.-i., High-brightness InGaN blue, green and yellow light-emitting diodes with quantum well structures. *Japanese J. App. Phys.* **1995**, *34* (7A), L797.

17. Shanmugam, M.; Jacobs-Gedrim, R.; Song, E. S.; Yu, B., Two-dimensional layered semiconductor/graphene heterostructures for solar photovoltaic applications. *Nanoscale* **2014**, *6* (21), 12682-12689.
18. Britnell, L.; Ribeiro, R.; Eckmann, A.; Jalil, R.; Belle, B.; Mishchenko, A.; Kim, Y.-J.; Gorbachev, R.; Georgiou, T.; Morozov, S. , Strong light-matter interactions in heterostructures of atomically thin films. *Science* **2013**, *340* (6138), 1311-1314.
19. Furchi, M. M.; Pospischil, A.; Libisch, F.; Burgdörfer, J.; Mueller, T., Photovoltaic effect in an electrically tunable van der Waals heterojunction. *Nano Lett.* **2014**, *14* (8), 4785-4791.
20. Dean, C. R.; Young, A. F.; Meric, I.; Lee, C.; Wang, L.; Sorgenfrei, S.; Watanabe, K.; Taniguchi, T.; Kim, P.; Shepard, K. L., Boron nitride substrates for high-quality graphene electronics. *Nature Nanotech.* **2010**, *5* (10), 722.
21. Zollner, K.; Junior, P. E. F.; Fabian, J., Proximity exchange effects in MoSe 2 and WSe 2 heterostructures with CrI 3: Twist angle, layer, and gate dependence. *Phys. Rev. B* **2019**, *100* (8), 085128.
22. Seyler, K. L.; Zhong, D.; Huang, B.; Linpeng, X.; Wilson, N. P.; Taniguchi, T.; Watanabe, K.; Yao, W.; Xiao, D.; McGuire, M. A., Valley manipulation by optically tuning the magnetic proximity effect in WSe<sub>2</sub>/CrI<sub>3</sub> heterostructures. *Nano Lett.* **2018**, *18* (6), 3823-3828.
23. Liu, Y.; Su, Y.; Guan, J.; Cao, J.; Zhang, R.; He, M.; Gao, K.; Zhou, L.; Jiang, Z. , 2D heterostructure membranes with sunlight-driven self-cleaning ability for highly efficient oil–water separation. *Adv. Func. Mat.* **2018**, *28* (13), 1706545.
24. Grigorenko, A.; Polini, M.; Novoselov, K., Graphene plasmonics. *Nature Photonics* **2012**, *6* (11), 749.
25. Withers, F.; Del Pozo-Zamudio, O.; Mishchenko, A.; Rooney, A.; Gholinia, A.; Watanabe, K.; Taniguchi, T.; Haigh, S.; Geim, A.; Tartakovskii, A., Light-emitting diodes by band-structure engineering in van der Waals heterostructures. *Nature Materials* **2015**, *14* (3), 301.
26. Yu, W. J.; Li, Z.; Zhou, H.; Chen, Y.; Wang, Y.; Huang, Y.; Duan, X., Vertically stacked multi-heterostructures of layered materials for logic transistors and complementary inverters. *Nature Materials* **2013**, *12* (3), 246.
27. Loan, P. T. K.; Zhang, W.; Lin, C. T.; Wei, K. H.; Li, L. J.; Chen, C. H., Graphene/MoS<sub>2</sub> heterostructures for ultrasensitive detection of DNA hybridisation. *Adv. materials* **2014**, *26* (28), 4838-4844.
28. Lee, G.-H.; Yu, Y.-J.; Cui, X.; Petrone, N.; Lee, C.-H.; Choi, M. S.; Lee, D.-Y.; Lee, C.; Yoo, W. J.; Watanabe, K., Flexible and transparent MoS<sub>2</sub> field-effect transistors on hexagonal boron nitride-graphene heterostructures. *ACS Nano* **2013**, *7* (9), 7931-7936.
29. Chiu, M.-H.; Zhang, C.; Shiu, H.-W.; Chuu, C.-P.; Chen, C.-H.; Chang, C.-Y. S.; Chen, C.-H.; Chou, M.-Y.; Shih, C.-K.; Li, L., Determination of band alignment in the single-layer MoS<sub>2</sub>/WSe<sub>2</sub> heterojunction. *Nature Communications* **2015**, *6*, 7666.
30. Wilson, N. R.; Nguyen, P. V.; Seyler, K.; Rivera, P.; Marsden, A. J.; Laker, Z. P.; Constantinescu, G. C.; Kandyba, V.; Barinov, A.; Hine, N. D., Determination of band offsets, hybridization, and exciton binding in 2D semiconductor heterostructures. *Sci. Adv.* **2017**, *3* (2), e1601832.
31. Andersen, K.; Latini, S.; Thygesen, K. S., Dielectric genome of van der Waals heterostructures. *Nano Lett.* **2015**, *15* (7), 4616-4621.
32. Mathew, K.; Singh, A. K.; Gabriel, J. J.; Choudhary, K.; Sinnott, S. B.; Davydov, A. V.; Tavazza, F.; Hennig, R. G., MPInterfaces: A Materials Project based Python tool for high-throughput computational screening of interfacial systems. *Computational Materials Science* **2016**, *122*, 183-190.
33. Ding, H.; Dwaraknath, S. S.; Garten, L.; Ndione, P.; Ginley, D.; Persson, K. A., Computational approach for epitaxial polymorph stabilization through substrate selection. *ACS App. Surf. Interfaces* **2016**, *8* (20), 13086-13093.

34. Zur, A.; McGill, T. J., Lattice match: An application to heteroepitaxy. *J. App. Phys.* **1984**, *55* (2), 378-386.
35. Choudhary, K.; Kalish, I.; Beams, R.; Tavazza, F., High-throughput Identification and Characterization of Two-dimensional Materials using Density functional theory. *Scientific Reports* **2017**, *7* (1), 5179.
36. Choudhary, K.; Cheon, G.; Reed, E.; Tavazza, F., Elastic properties of bulk and low-dimensional materials using van der Waals density functional. *Physical Review B* **2018**, *98* (1), 014107.
37. Choudhary, K.; Zhang, Q.; Reid, A. C.; Chowdhury, S.; Van Nguyen, N.; Trautt, Z.; Newrock, M. W.; Congo, F. Y.; Tavazza, F., Computational screening of high-performance optoelectronic materials using OptB88vdW and TB-mBJ formalisms. *Scientific data* **2018**, *5*, 180082.
38. Choudhary, K.; Bercx, M.; Jiang, J.; Pachter, R.; Lamoén, D.; Tavazza, F., Accelerated Discovery of Efficient Solar-cell Materials using Quantum and Machine-learning Methods. *Chemistry of Materials* **2019**.
39. Choudhary, K.; Garrity, K. F.; Tavazza, F. High-throughput Discovery of Topologically Non-trivial Materials using Spin-orbit Spillage. *Scientific Reports* **2019**, *9* (1), 8534.
40. Haastrup, S.; Strange, M.; Pandey, M.; Deilmann, T.; Schmidt, P. S.; Hinsche, N. F.; Gjerding, M. N.; Torelli, D.; Larsen, P. M.; Riis-Jensen, A., The Computational 2D Materials Database: high-throughput modeling and discovery of atomically thin crystals. *2D materials* **2018**, *5* (4), 042002.
41. Geim, A. K.; Grigorieva, I. V., Van der Waals heterostructures. *Nature* **2013**, *499* (7459), 419.
42. Kang, J.; Li, J.; Li, S.-S.; Xia, J.-B.; Wang, L.-W., Electronic structural Moiré pattern effects on MoS<sub>2</sub>/MoSe<sub>2</sub> 2D heterostructures. *Nano Lett.* **2013**, *13* (11), 5485-5490.
43. Choudhary, K.; DeCost, B.; Tavazza, F., Machine learning with force-field-inspired descriptors for materials: Fast screening and mapping energy landscape. *Physical Review Materials* **2018**, *2* (8), 083801.
44. Kresse, G.; Furthmüller, J., Efficient iterative schemes for ab initio total-energy calculations using a plane-wave basis set. *Phys. Rev. B* **1996**, *54* (16), 11169.
45. Kresse, G.; Furthmüller, J., Efficiency of ab-initio total energy calculations for metals and semiconductors using a plane-wave basis set. *Comp.Mat. Sci.* **1996**, *6* (1), 15-50.
46. Klimeš, J.; Bowler, D. R.; Michaelides, A. J., Chemical accuracy for the van der Waals density functional. *J. Phys. Cond. Matt.* **2009**, *22* (2), 022201.
47. Grinberg, M., *Flask web development: developing web applications with python*. "O'Reilly Media, Inc.": 2018.
48. Ke, G.; Meng, Q.; Finley, T.; Wang, T.; Chen, W.; Ma, W.; Ye, Q.; Liu, T.-Y. In *Lightgbm: A highly efficient gradient boosting decision tree*, Advances in Neural Information Processing Systems, 2017; pp 3146-3154.
49. Kroemer, H., Heterostructure devices: A device physicist looks at interfaces. In *Electronic Structure of Semiconductor Heterojunctions*, Springer: 1988; pp 116-149.
50. Bellus, M. Z.; Li, M.; Lane, S. D.; Ceballos, F.; Cui, Q.; Zeng, X. C.; Zhao, H., Type-I van der Waals heterostructure formed by MoS<sub>2</sub> and ReS<sub>2</sub> monolayers. *Nanoscale* **2017**, *2* (1), 31-36.
51. Xiao, J.; Zhang, Y.; Chen, H.; Xu, N.; Deng, S., Enhanced Performance of a Monolayer MoS<sub>2</sub>/WSe<sub>2</sub> Heterojunction as a Photoelectrochemical Cathode. *Nano-micro lett.* **2018**, *10* (4), 60.
52. Yan, X.; Liu, C.; Li, C.; Bao, W.; Ding, S.; Zhang, D. W.; Zhou, P., Tunable SnSe<sub>2</sub>/WSe<sub>2</sub> heterostructure tunneling field effect transistor. *Small* **2017**, *13* (34), 1701478.
53. Sarkar, D.; Xie, X.; Liu, W.; Cao, W.; Kang, J.; Gong, Y.; Kraemer, S.; Ajayan, P. M.; Banerjee, K. J. N., A subthermionic tunnel field-effect transistor with an atomically thin channel. **2015**, *526* (7571), 91.
54. Rahman, M. Z.; Kwong, C. W.; Davey, K.; Qiao, S. Z., 2D phosphorene as a water splitting photocatalyst: fundamentals to applications. *Eng and Env. Sci.* **2016**, *9* (3), 709-728.
55. Luo, B.; Liu, G.; Wang, L., Recent advances in 2D materials for photocatalysis. *Nanoscale* **2016**, *8* (13), 6904-6920.

56. Wang, N.; Yang, G.; Wang, H.; Sun, R.; Wong, C.-P., Visible Light-Responsive Photocatalytic Activity of Boron Nitride Incorporated Composites. *Frontiers in Chem.* **2018**, *6*.
57. Du, C.-F.; Liang, Q.; Dangol, R.; Zhao, J.; Ren, H.; Madhavi, S.; Yan, Q., Layered trichalcogenidophosphate: a new catalyst family for water splitting. *Nano-micro Lett.* **2018**, *10* (4), 67.
58. Sholl, D.; Steckel, J. A., *Density functional theory: a practical introduction*. John Wiley & Sons: 2011.
59. Hummer, K.; Harl, J.; Kresse, G., Heyd-Scuseria-Ernzerhof hybrid functional for calculating the lattice dynamics of semiconductors. *Phys. Rev. B* **2009**, *80* (11), 115205.
60. Heyd, J.; Scuseria, G. E.; Ernzerhof, M. J. T., Hybrid functionals based on a screened Coulomb potential. *J. Chem. Phys.* **2003**, *118* (18), 8207-8215.
61. Shishkin, M.; Kresse, G., Implementation and performance of the frequency-dependent G W method within the PAW framework. *Phys. Rev. B* **2006**, *74* (3), 035101.
62. Shishkin, M.; Kresse, G., Self-consistent G W calculations for semiconductors and insulators. *Phys. Rev. B* **2007**, *75* (23), 235102.
63. Burke, K., *The ABC of DFT. Department of Chemistry, University of California* **2007**.